Electronic Supplementary Material (ESI) for Journal of Materials Chemistry A.

Supporting Information:

A Liquid-Crystalline Non-Fullerene Acceptor Enabling High-Performance Organic Solar Cells

Pierluigi Mondelli,[a,c] Francesco Silvestri,[b] Laura Ciammaruchi,[b] Eduardo Solano,[d] Eduardo Beltrán-Gracia,[c] Esther Barrena,[b] Moritz Riede[a] and Graham Morse[*c]

a. Clarendon Laboratory, University of Oxford, Parks Road, Oxford, OX1 3PU, United Kingdom.

b. Institut de Ciència de Materials de Barcelona, ICMAB-CSIC, Campus UAB, 08193 Bellaterra, Spain.

c. Merck Chemicals Ltd, Chilworth Technical Centre, University Parkway, Southampton, SO16 7QD, United Kingdom.

Email: graham.morse@gmail.com

d. ALBA Synchrotron Light Source, NCD-SWEET Beamline, Cerdanyola del Valles, 08290 Spain.

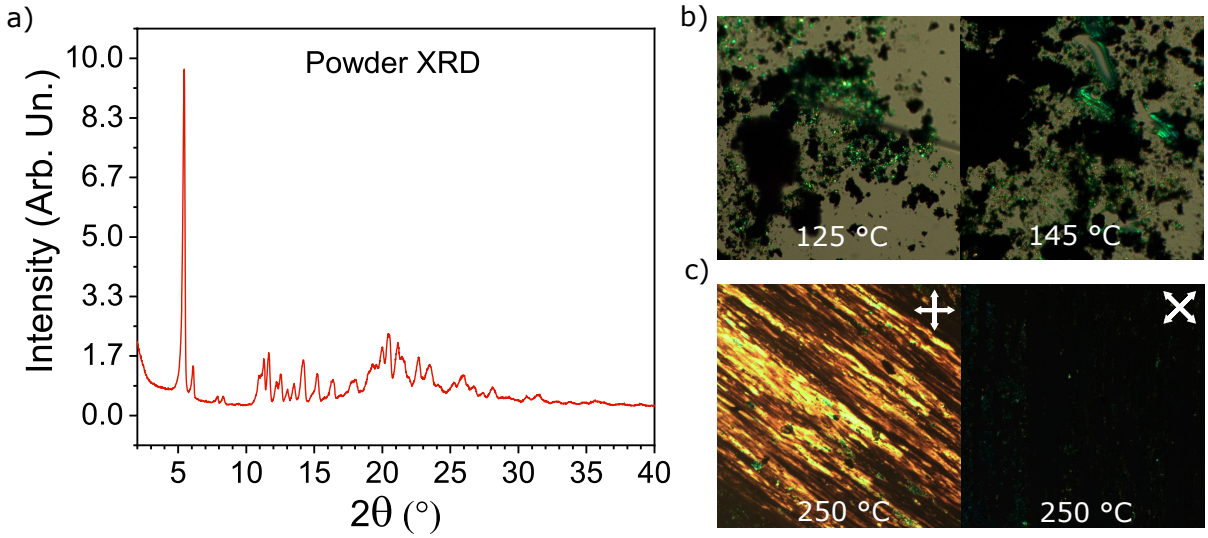

Figure S1 a) 4TICO Powder XRD showing the material crystallinity at room temperature. Right panel: optical images acquired in transmission mode on a 4TICO powder sample placed on the heating stage. b) The sample is crystalline and highly viscous until 145 °C, when the ϕ1 liquid phase is being formed. Crossed-polarized images (c) indicate a clear birefringence from aligned domains upon shearing stress at 250 °C.

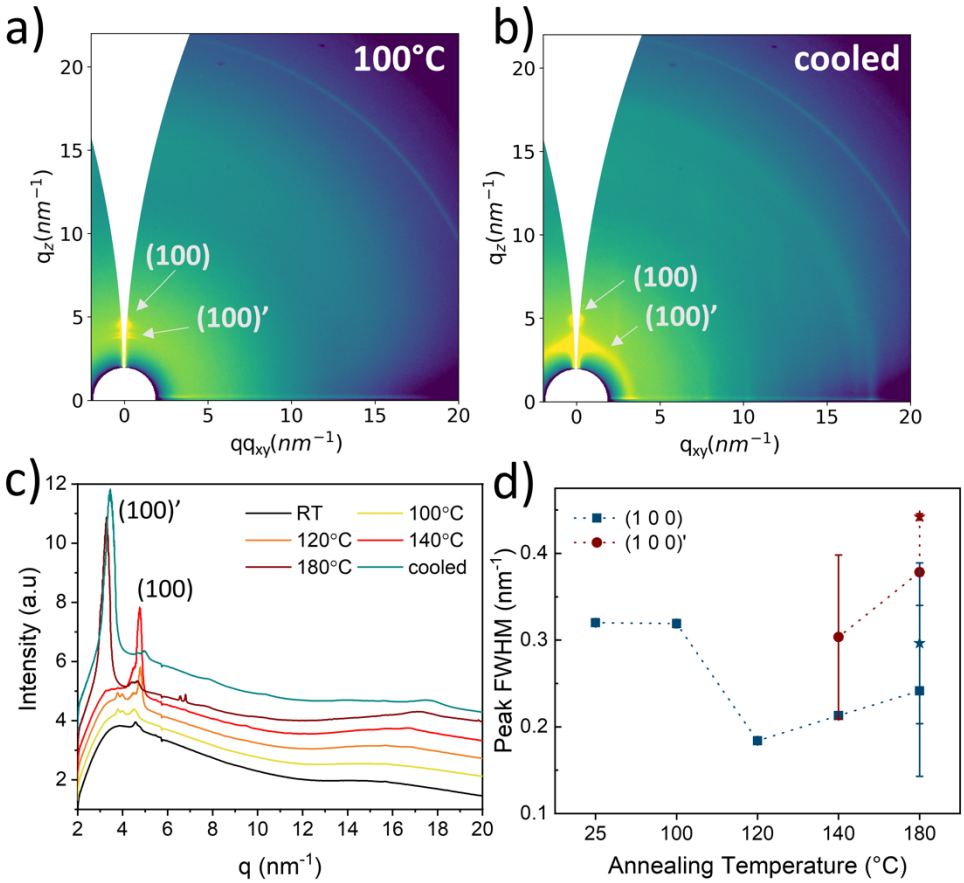

Figure S2 Complementary 2D GIWAXS maps of the 4TICO film at (a) 100°C and (b) after cooling down. (c) Evolution of the 1D integration profiles with at annealing at all the temperatures and (d) FWHM evolution of the lamellar features of the low-temperature (blue) and high-temperature (red) polymorphs, obtained from the OOP data.

From the FWHM (Δq), the crystalline coherence length (CL) is estimated by using the approximated expression of the Scherrer equation, CL = 2π/ Δq. Although the Scherrer equation works with the assumption that the crystallite size is the main contributor to the broadening of diffraction peaks while lattice disorder is ignored1, it can still give descriptive evidence for relative changes when processing conditions are varied experimentally.

In this sense, the exact value of the constant K in the Scherrer equation, CL = 2π K /Δq, being close to one, has little significance (K is a shape factor, typically 0.8–1).1, 2

For the (100) (polymorph I), the CL almost doubles from 20 nm up to 35 nm at 120°C to then lower to about 27 nm at 180°C. For the LC phase, the CL derived from the (100)' peak goes from 21 to 16 nm when annealing from 140°C to 180°C.

Temp (°C)	(100)		(200)		(100)'		π-π'	
	q_c (nm^{-1})	d (nm)	q_c (nm^{-1})	d (nm)	q_c (nm^{-1})	d (nm)	q_c (nm^{-1})	d (nm)
25	4.6	1.4	9.3	0.7	-	-	-	-
100	4.5	1.4	9.0	0.7	-	-	-	-
120	4.8	1.3	9.5	0.7	-	-	-	-
140	4.7	1.3	9.4	0.7	3.2	1.9	16.6	0.4
180	4.6	1.4	9.8	0.6	3.2	1.9	17.5	0.4
cooled	5.0	1.3	10.0	0.6	3.4	1.8	17.4	0.4

Table S1 OOP positions (q_c) and corresponding spacings (d) of the main periodicities assigned to the 4TICO from the 2D-GIWAXS in-situ experiment.

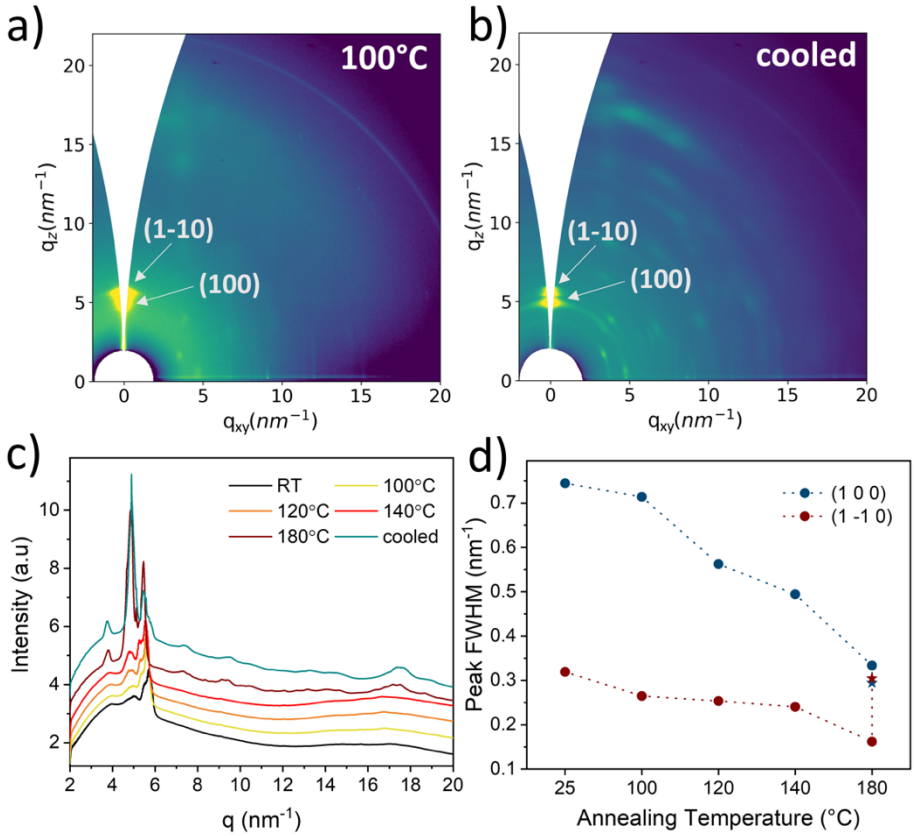

Figure S3 Complementary 2D GIWAXS maps of the 4TIC film at (a) 100°C and (b) after cooling down. (c) Evolution of the 1D integration profiles with at annealing at all the temperatures and (d) FWHM evolution of the two main features (from OOP data).

In this case a gradual increase of the CL is observed with annealing temperature. Considering the (100) peak, the CL goes from about 8 nm at RT up to 19 nm at 180°C.

Temp (°C)	(100)		(-110)	
	q_c (nm^{-1})	d (nm)	q_c (nm^{-1})	d (nm)
25	5.0	1.2	5.7	1.1
100	5.0	1.3	5.6	1.1
120	4.9	1.3	5.6	1.1
140	4.8	1.3	5.6	1.1
180	4.8	1.3	5.5	1.2
cooled	4.9	1.3	5.7	1.1

Table S1 OOP positions (q_c) and corresponding spacings (d) of the main periodicities assigned to the 4TIC from the 2D-GIWAXS in-situ experiment.

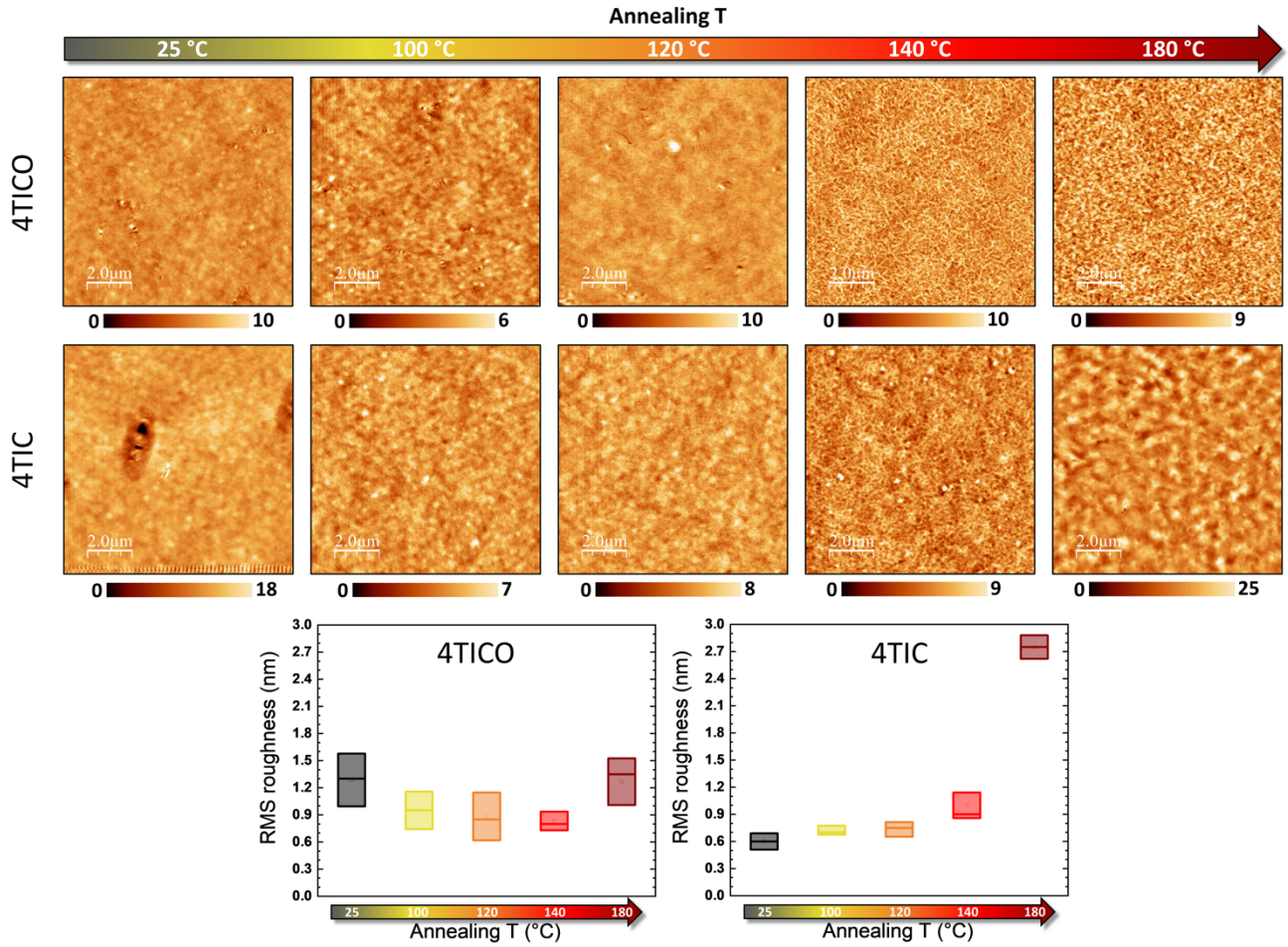

Figure S4. Morphological evolution of the 4TICO and 4TIC films upon annealing: 10x10 µm2 AFM topography images; the reported colour scale bars are in nanometres. At the bottom the root mean square (rms) roughness evolution with annealing is reported for the two materials.

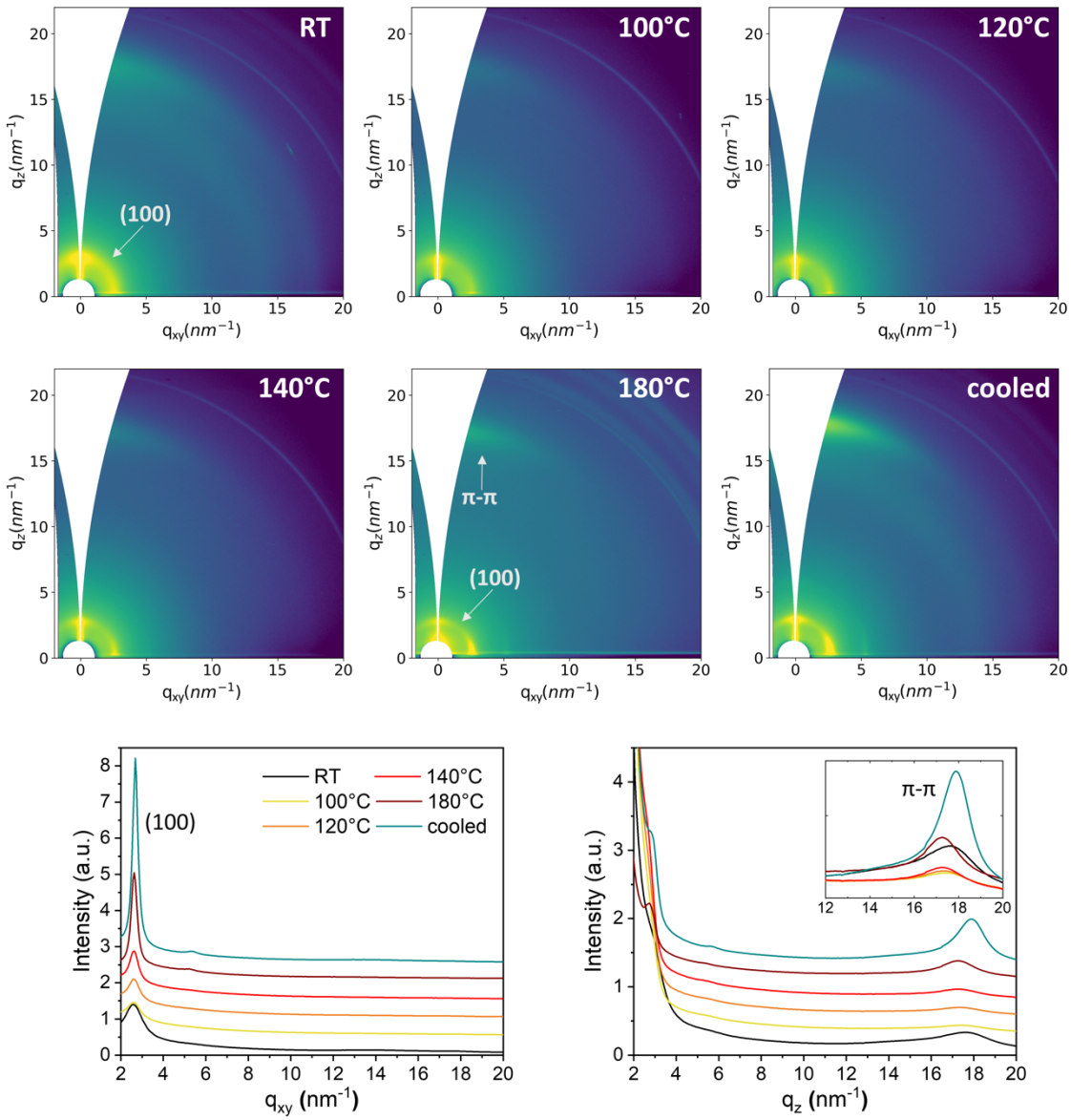

Figure S5 2D GIWAXS maps showing the structural evolution of the PBTZT-stat-BDTT-8 film at all the steps of the thermal annealing. At the bottom, the in-plane (IP) and out-of-plane (OOP) profiles are reported.

Temp (°C)	(100)		π-π	
	q_c (nm^{-1})	d (nm)	q_c (nm^{-1})	d (nm)
25	-	-	17.7	0.4
100	2.7	2.3	17.5	0.4
120	2.7	2.3	17.4	0.4
140	2.7	2.3	17.3	0.4
180	2.8	2.3	17.3	0.4
cooled	2.9	2.2	17.9	0.4

Table S3 OOP positions (q_c) and corresponding spacings (d) of the main periodicities assigned to the PBTZT-stat-BDTT-8 from the 2D-GIWAXS in-situ experiment.

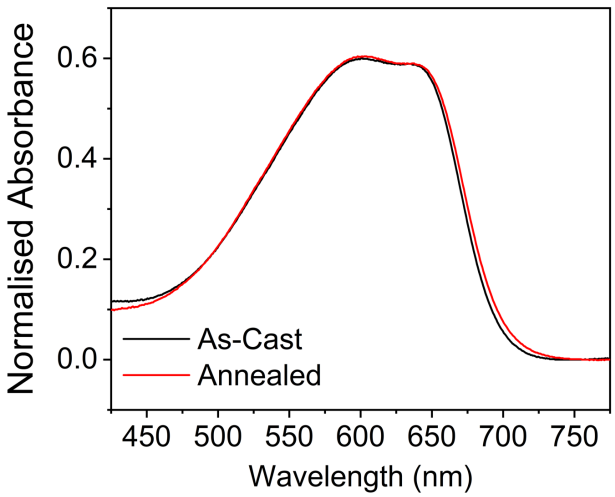

Figure S6 UV-vis absorption spectra acquired on PBTZT-stat-BDTT-8 as-cast and 140°C annealed films.

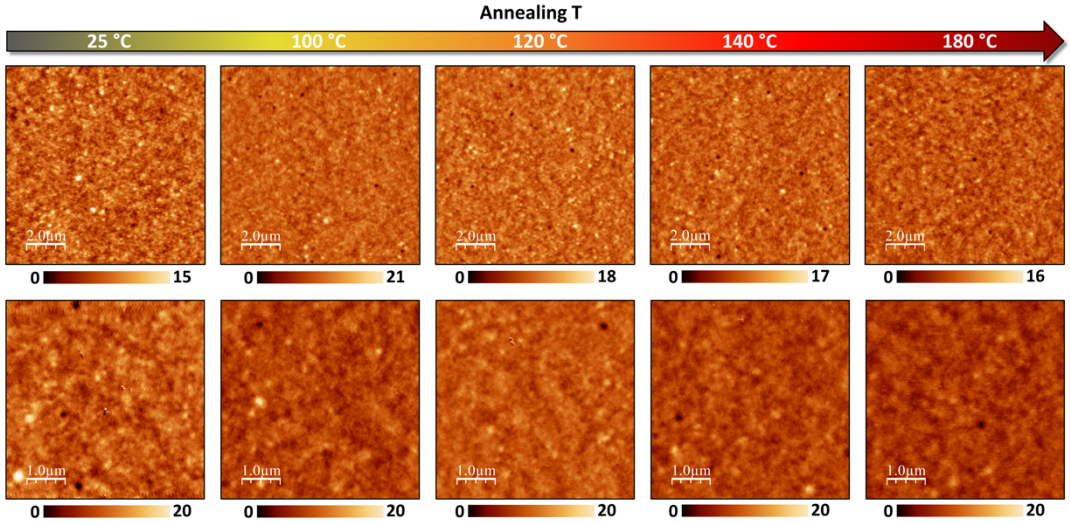

Figure S7 Morphological evolution of the PBTZT-stat-BDTT-8 film upon annealing: 10x10 µm2 (top) and 5x5 µm2 (bottom) AFM topography images; the reported colour scale bars are in nanometres.

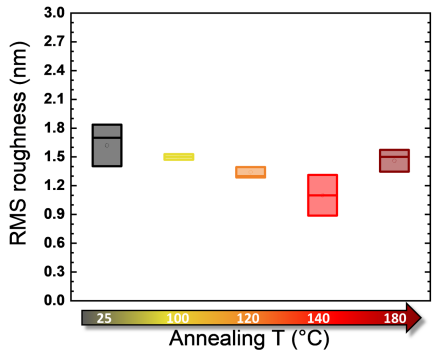

Figure S8. Root mean square (rms) roughness evolution with annealing for the PBTZT-stat-BDTT-8 film.

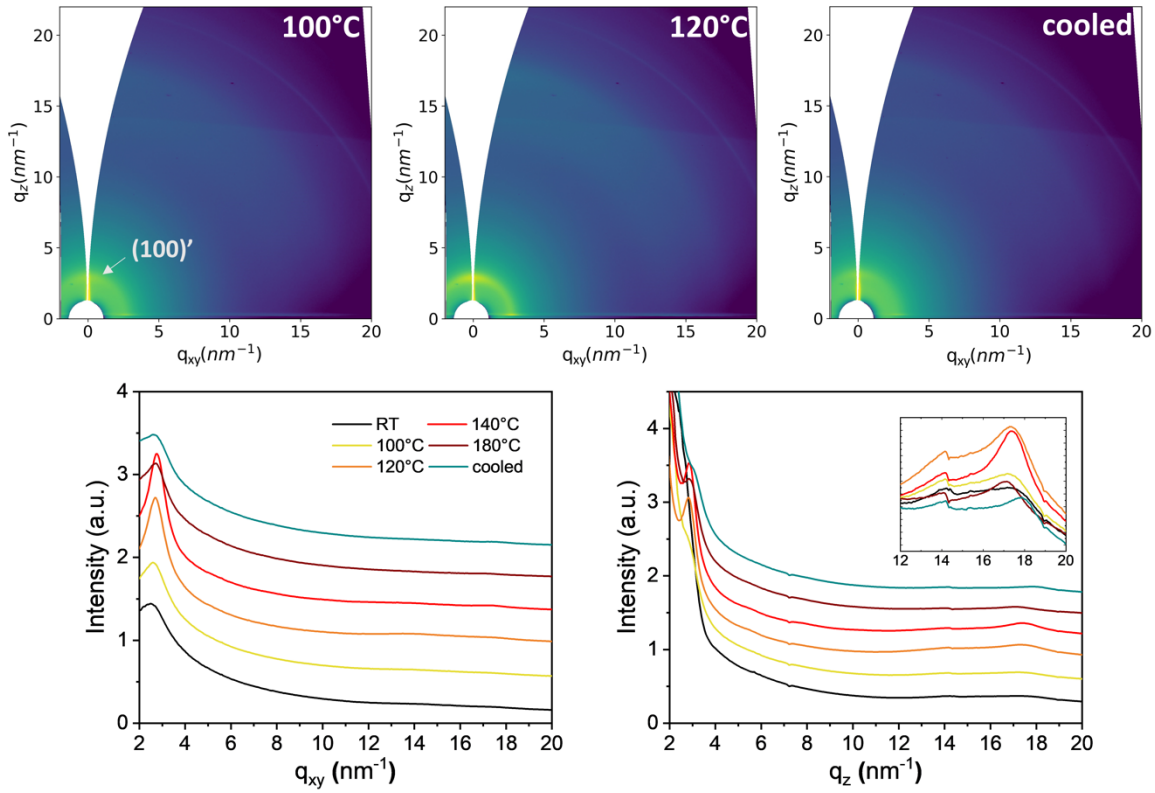

Figure S9 Complementary 2D GIWAXS maps of the PBTZT-stat-BDTT-8:4TICO blend at 100°C, 120°C and after cooling down. At the bottom, the in-plane (IP) and out-of-plane (OOP) profiles are reported.

Temp (°C)	(100)'	
	q_c (nm^{-1})	d (nm)
25	-	-
100	3.0	2.1
120	2.9	2.2
140	2.9	2.1
180	3.0	2.1
cooled	3.2	2.0

Table S4. OOP positions (q_c) and corresponding spacings (d) of the main periodicities observed in the PBTZT-stat-BDTT-8:4TICO blend from the 2D-GIWAXS in-situ experiment.

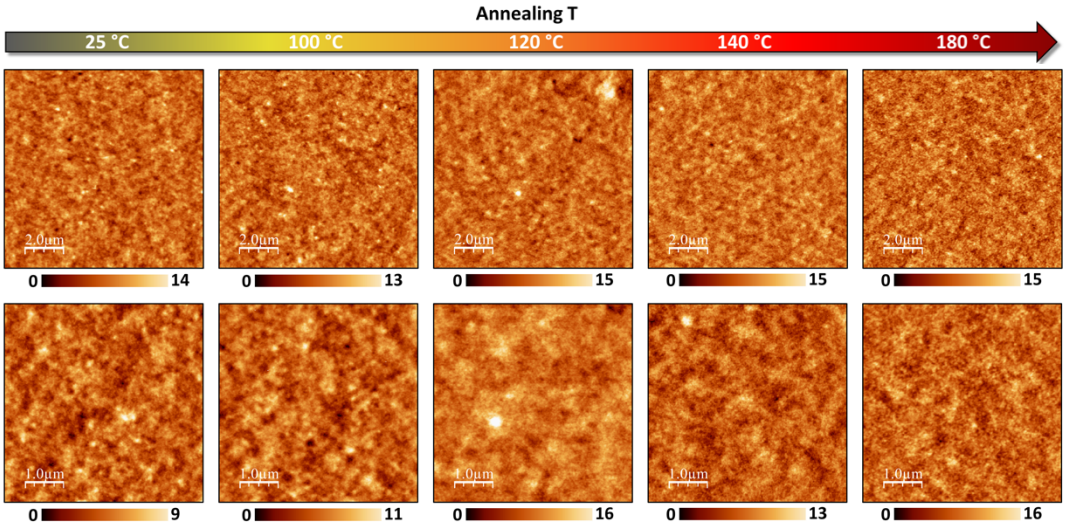

Figure S10 Morphological evolution of the PBTZT-stat-BDTT-8:4TICO blend upon annealing: 10x10 µm2 (top) and 5x5 µm2 (bottom) AFM topography images; the reported colour scale bars are in nanometres.

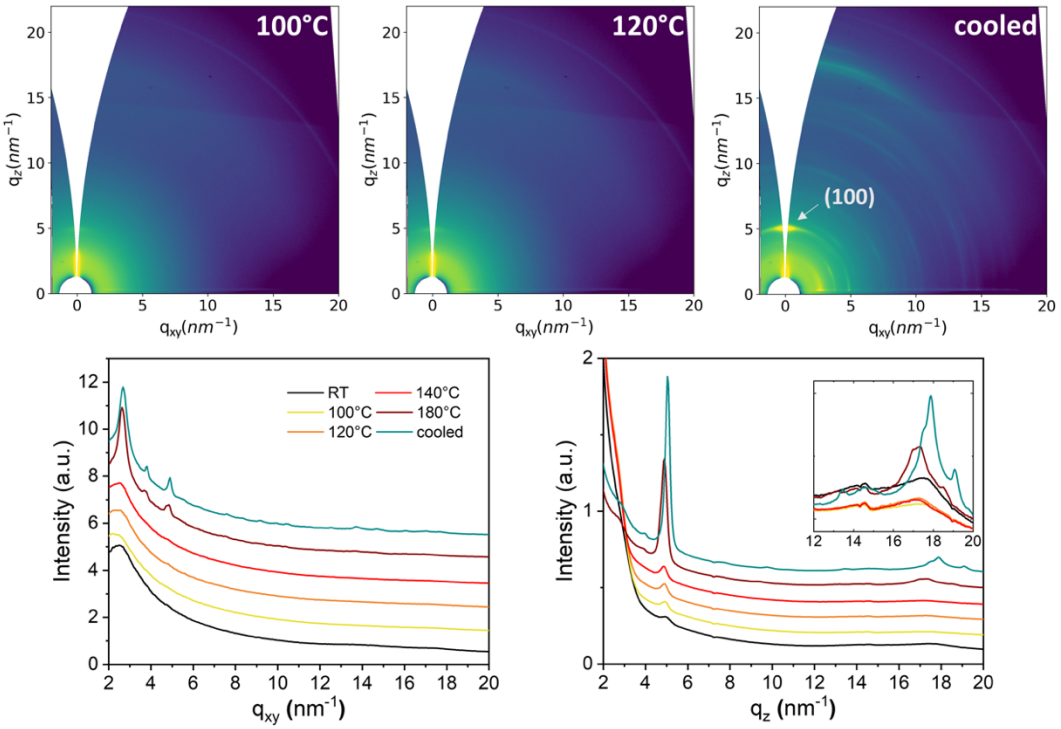

Figure S11. Complementary 2D GIWAXS maps of the PBTZT-stat-BDTT-8:4TIC blend at 100°C, 120°C and after cooling down. At the bottom, the in-plane (IP) and out-of-plane (OOP) profiles are reported.

Temp (°C)	$(100)_D$		$(100)_A$	
	q_c (nm^{-1})	d (nm)	q_c (nm^{-1})	d (nm)
25	2.8	2.2	5.0	1.3
100	2.7	2.3	4.9	1.3
120	2.7	2.3	4.9	1.3
140	2.6	2.4	4.9	1.3
180	2.7	2.3	4.9	1.3
cooled	2.8	2.3	5.0	1.2

Table S5. OOP positions (q_c) and corresponding spacings (d) of the main periodicities of the donor (D) and acceptor (A) materials observed in the PBTZT-stat-BDTT-8:4TIC blend from the 2D-GIWAXS in-situ experiment.

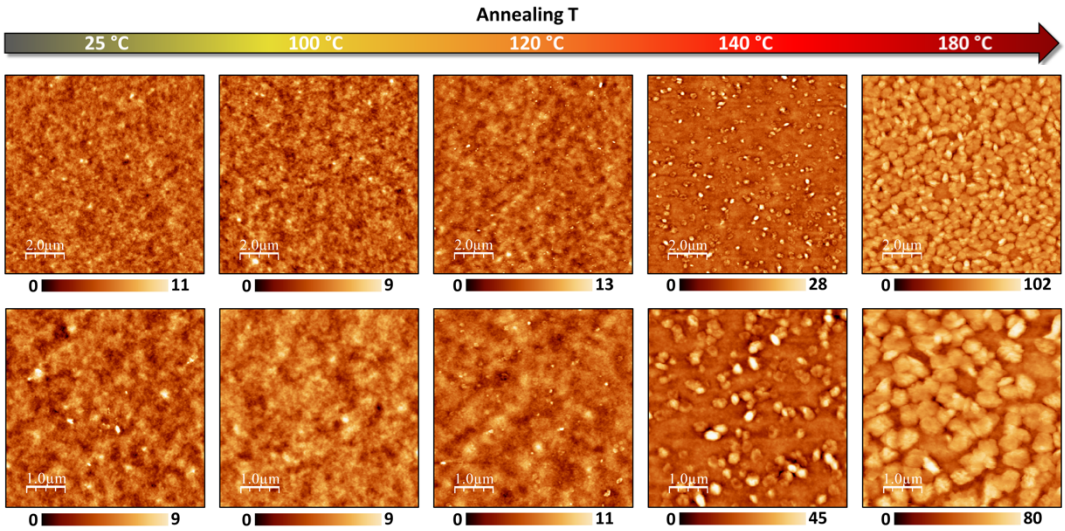

Figure S12. Morphological evolution of the PBTZT-stat-BDTT-8:4TIC blends upon annealing: 10x10 µm² (top) and 5x5 µm² (bottom) AFM topography images; the reported colour scale bars are in nanometres.

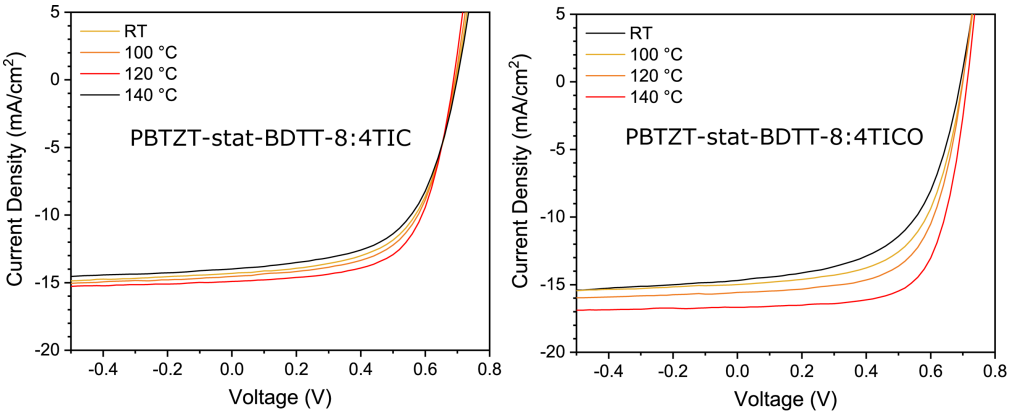

Figure S13 Evolution of the JV curve after each annealing step.

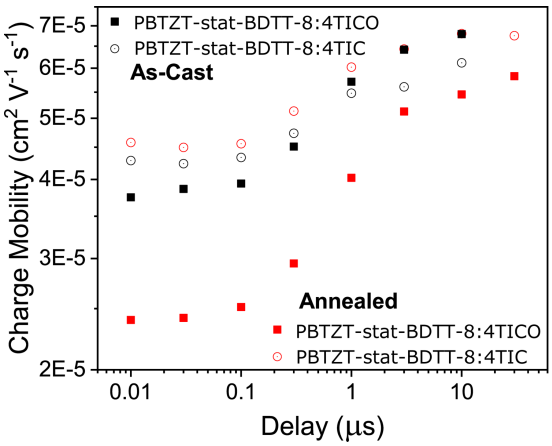

Figure S14 Charge mobility calculated under different delay times.

References

1. J. Rivnay, R. Noriega, R. J. Kline, A. Salleo and M. F. Toney, *Physical Review B*, 2011, **84**, 045203.
2. B. E. Warren, *X-ray Diffraction*, Courier Corporation, 1990.